Identification of substorm onset location and preonset sequence using Reimei, THEMIS GBO, PFISR, and Geotail

S. Zou,[1] M. B. Moldwin,[1] L. R. Lyons,[2] Y. Nishimura,[2,3] M. Hirahara,[4] T. Sakanoi,[5] K. Asamura,[6] M. J. Nicolls,[7] Y. Miyashita,[3] S. B. Mende,[8] and C. J. Heinselman[7]

Received 30 March 2010; revised 16 September 2010; accepted 4 October 2010; published 7 December 2010.

[1] We present state-of-the-art multiple instrument observations of an isolated substorm on October 12, 2007. The auroral breakup was observed simultaneously by Reimei, THEMIS ASI, and PFISR. The footprint of Geotail was also near the breakup. These observations allow for detailed study of the breakup location in terms of large- and small-scale auroral morphology, particle precipitation, and ionospheric convection, which has not previously been achieved. It also allows for detailed identification of the sequence leading to the breakup. We report the first spaceborne high spatial and temporal resolution images of part of a breakup arc and a wave-like auroral enhancement captured by Reimei. Observations suggest a sudden plasma sheet thinning initiated ~10 min before the onset. Wave-like auroral enhancements were observed twice at the most equatorward arc ~3 min and ~1 min before the breakup. These enhancements are likely due to some near-Earth instability, such as ballooning instability. Unlike the usual substorm sequence, this most equatorward arc did not develop into the breakup arc but remained almost stable until being engulfed by the auroral equatorward expansion from higher latitude after onset. The wave-like auroral enhancement was associated with three fine inverted V arcs and embedded within energetic ion precipitation. Following this enhancement, an arc, likely a poleward boundary intensification, formed at higher latitude just adjacent to the plasma sheet boundary layer (PSBL). This arc then extended southwestward and led to the breakup arc, which was located poleward of the wavy structures. Assuming longitudinal homogeneity of ion precipitation over 1°, this breakup arc was located in a region without ion precipitation just poleward of the energetic ion precipitation. These observations suggest the possible existence of a low-entropy flow channel associated with the arc adjacent to the PSBL, which might be associated with instability in the near-Earth plasma sheet responsible for the auroral breakup.

Citation: Zou, S., et al. (2010), Identification of substorm onset location and preonset sequence using Reimei, THEMIS GBO, PFISR, and Geotail, *J. Geophys. Res.*, *115*, A12309, doi:10.1029/2010JA015520.

1. Introduction

[2] Substorms are one of the fundamental elements of geomagnetic activity. They include global-scale reconfigurations of the magnetosphere and can be accompanied by spectacular aurora. In the ionosphere, sudden brightening of an arc, often the most equatorward one, extending a few thousand kilometers in the east-west direction near midnight, either a preexisting one or a newly formed one, has been frequently used to identify the location and time of substorm onset [*Akasofu*, 1964]. After onset, the brightened arc rapidly expands poleward and azimuthally, i.e., breakup, and forms the auroral bulge and westward traveling surge (WTS) [*Akasofu et al.*, 1965, 1966]. The WTS is the western terminator of the bulge and is often associated with an auroral spiral rotating clockwise [*Paschmann et al.*, 2002]. In spite of this well-known substorm sequence, the physical mechanism that leads to substorm onset and the subsequent explosive expansion remains a controversial topic even four decades after the discovery of the substorm.

[3] Current substorm models can be approximately divided into two categories: inside-out or outside-in, in terms of

[1]Department of Atmospheric, Oceanic and Space Sciences, University of Michigan, Ann Arbor, Michigan, USA.
[2]Department of Atmospheric and Oceanic Sciences, University of California, Los Angeles, California, USA.
[3]Solar-Terrestrial Environment Laboratory, Nagoya University, Nagoya, Japan.
[4]Department of Earth and Planetary Science, University of Tokyo, Tokyo, Japan.
[5]Planetary Plasma and Atmospheric Research Center, Tohoku University, Sendai, Japan.
[6]Institute of Space and Astronautical Science, Sagamihara, Japan.
[7]Center for Geospace Studies, SRI International, Menlo Park, California, USA.
[8]Space Sciences Laboratory, University of California, Berkeley, California, USA.

0148-0227/10/2010JA015520

propagation direction of events in the magnetotail that initiates the substorm onset. The inside-out model predicts that near-Earth (less than ~10 *Re* downtail) plasma instability disrupts the cross-tail current and then causes the arc brightening [*Lui et al.*, 1992; *Lyons*, 1995; *Cheng and Lui*, 1998; *Erickson et al.*, 2000; *Lui*, 2004, and references therein; *Cheng*, 2004, and references therein]. The rarefaction wave caused by the current disruption then propagates tailward and may set up favorable conditions for reconnection at ~20–30 *Re* downtail to occur. In contrast, in the outside-in model, magnetic reconnection at 20–30 *Re* in the tail occurs first [e.g., *Baker et al.*, 1996; *Angelopoulos et al.*, 2008] and launches earthward and tailward fast flows [*Nagai et al.*, 1998; *Miyashita et al.*, 2000]. The fast earthward flow bursts brake and divert in the near-Earth region, leading to the formation of substorm current wedge and the brightening of the auroral arc [*Shiokawa et al.*, 1997]. *Ohtani* [2001] pointed out that understanding how the two processes (current disruption and reconnection) are physically related is the most important question for substorm studies.

[4] *Kepko et al.* [2009] reported a substorm event in which a 630.0 nm diffuse auroral patch moved equatorward and reached the onset arc at the onset time. This diffuse auroral patch was suggested to be associated with an earthward moving flow burst and supports the outside-in model. Recently, *Nishimura et al.* [2010] found a repeatable sequence of events that often leads to substorm onset, the sequence having some features of previous inside-out and outside-in models. An auroral streamer developing from a poleward boundary intensification (PBI) propagates equatorward and touches an arc further equatorward near the Harang flow reversal and then the onset occurs. The authors suggested that "low-entropy flow channels" associated with enhanced reconnection near the polar cap boundary divert at the Harang reversal and initiate a near-Earth instability that leads to onset. Such low-entropy flow channels are sometimes referred to as "bubbles" to describe an earthward moving flux tube with lower entropy parameter ($PV^{5/3}$) than the surrounding region [*Pontius and Wolf*, 1990; *Chen and Wolf*, 1993]. Here P is the particle thermal pressure and V is the flux tube volume for a closed magnetic field line. This concept has been adapted to explain fast flow bursts in the plasma sheet [*Chen and Wolf*, 1993; *Sergeev et al.*, 1996]. Characteristics of plasma within the low-entropy channel include higher plasma speed, lower particle number density, and larger magnetic Bz component in the equatorial plane [e.g., *Sergeev et al.*, 1996; *Wolf et al.*, 2009]. Under the assumption of strong pitch angle scattering, a highly depleted channel is expected to connect to regions of reduced particle precipitation and thus low conductance in the ionosphere [*Wolf et al.*, 2009].

[5] The onset controversy is due in part to the limitation of observational capability. Given a limited number of satellites in the magnetosphere, it is difficult to determine exactly where and when the substorm onset initiates or the 2-D distribution of important physical quantities. Remote sensing of the ionospheric manifestations of substorms, such as the breakup arc, offers an opportunity to locate the onset relative to large-scale auroral morphology, particle precipitation and convection.

[6] Simultaneous high temporal and spatial resolution particle and optical measurements are essential for unambiguous determination of the characteristics of precipitating particles and the resulting auroral arcs. This requires either conjunction observations by ground-based optical instruments and spaceborne particle detectors, or by a satellite equipped with both imager and particle detectors. However, in both cases, it is extremely rare to have such observations at the onset location and within a couple of minutes of onset. The rareness can be attributed to multiple factors, such as present poor ability of forecasting the occurrence of substorms, clear skies required by ground-based optical all-sky imaging (ASI) observations, the limited field of view (FOV) of high spatial resolution satellite-based auroral imaging, and more importantly the transient and localized nature of the breakup arc.

[7] Only a limited number of studies in the literature report simultaneous particle and optical observations near onset location within a couple of minutes of onset [*Dubyagin et al.*, 2003; *Mende et al.*, 2003]. *Dubyagin et al.* [2003] reported FAST and ASI with 20 s cadence observations of the most equatorward arc just prior to its breakup. They found that this was an inverted V arc located only ~0.4° poleward of the proton isotropic boundary, in the region of a strong earthward pressure gradient, and at ~8 R_E in the equatorial plane based on the Tyganenko 96 model. By using the FAST and IMAGE satellite observations obtained ~2 min after the onset, *Mende et al.* [2003] found that the most intense onset poleward surge was generated by superthermal electrons associated with Alfvén waves and was located in a region of energetic ion precipitation.

[8] In addition, *Yago et al.* [2005, 2007] reported simultaneous DMSP and ASI observations of the brightening arc for two pseudobreakups, and in both cases the arcs were associated with an inverted V structure at the equatorward edge of the electron precipitation region and at the poleward boundary of the energetic (>1 keV) ion precipitation region. *Shiokawa et al.* [2005] presented DMSP observations of the particle precipitation responsible for the leading edge of WTS captured simultaneously by IMAGE and an ASI 1–2 h in magnetic local time (MLT) west of onset. These authors found that the arcs are associated with electron inverted V precipitation at the equatorward boundary of the Region 1 type upward field-aligned current (FAC) region, and within the sunward convection region.

[9] In this paper, we present a detailed high temporal resolution study of a substorm onset on 12 October 2007 using simultaneous observations from the THEMIS ASI, Reimei satellite, PFISR radar and Geotail satellite. Reimei captured a portion of the breakup arc at the time of the initiation. Observations from these instruments are presented in section 2. We discuss the implications of the sequences of events observed near the onset time in section 3 and summarize key observations in section 4.

2. Observations

[10] On 12 October 2007, a substorm onset occurred at 1119:42 UT over central Alaska. The provisional AU/AL indices (not shown) show no evidence for substorm activity for the previous several hours, indicating this was an isolated substorm event.

2.1. Interplanetary Observations

[11] Figure 1 shows the solar wind and interplanetary magnetic field (IMF) observations in GSM coordinates from

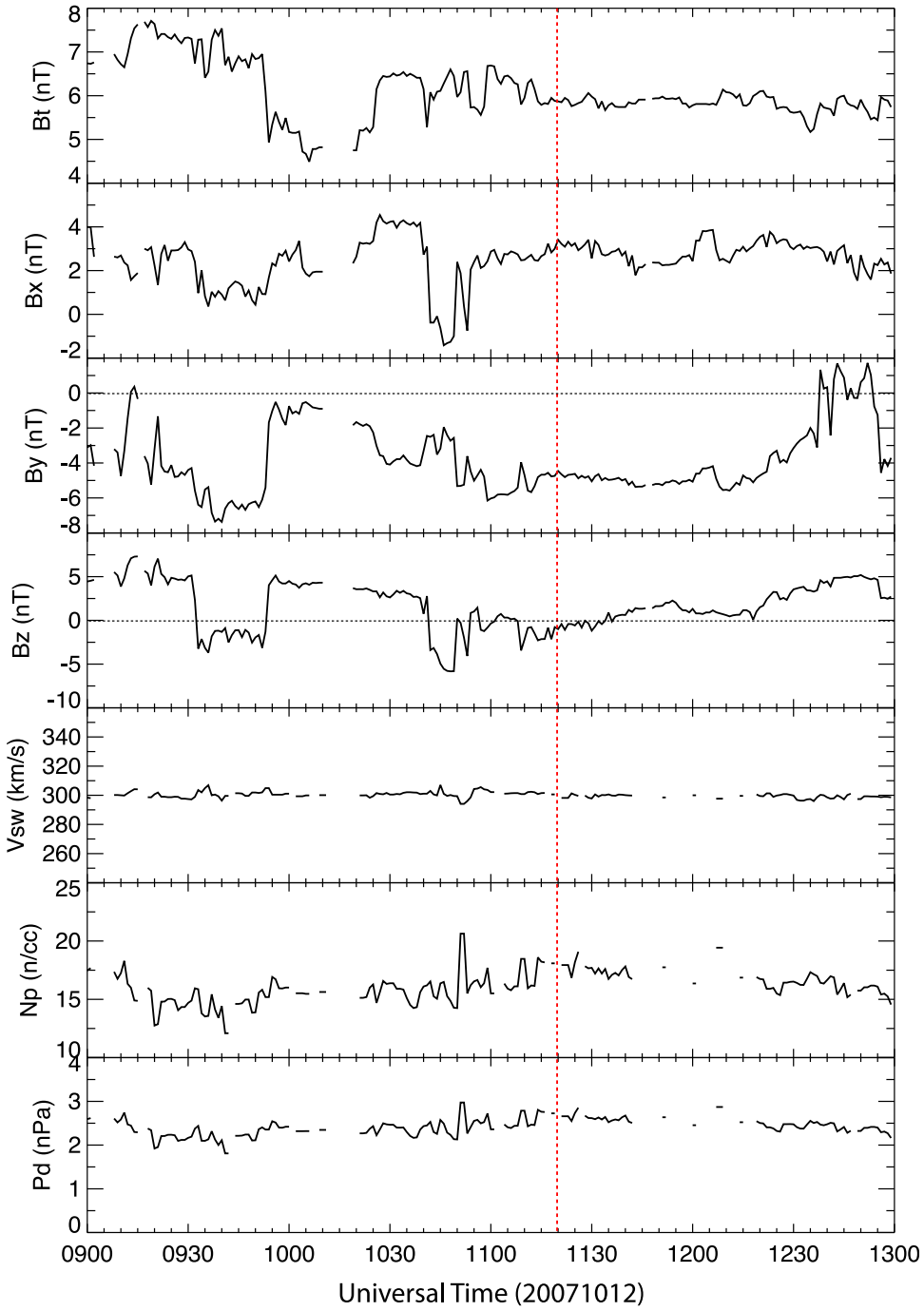

Figure 1. IMF and solar wind observations from 0900 to 1300 UT in the GSM coordinates. (top to bottom) Time series of the total magnetic field (B*t*), IMF B*x*, B*y*, B*z*, solar wind speed (V*sw*), proton number density (N*p*), and dynamic pressure (P*d*) are shown. The vertical line indicates the substorm onset time determined by the THEMIS ASI observations.

09 to 13 UT with 1 min temporal resolution, which are obtained from the OMNI website (http://omniweb.gsfc.nasa.gov/) and are time shifted to the nose of the bow shock. From top to bottom, time series of the total magnetic field (B*t*), IMF B*x*, B*y*, B*z*, solar wind speed (V*sw*), proton number density (N*p*) and dynamic pressure (P*d*) are shown. The vertical line indicates the substorm onset time determined based on THEMIS ASI observations, which are described in the next section. Within the hour before substorm onset, the IMF *Bz* was northward or weakly southward with a ~10 min excursion to ~–5 nT about 40 min before the onset and the IMF *By* was increasingly negative to ~–6 nT just before onset, which is likely responsible for the postmidnight onset location at ~0.6 MLT in this case, consistent with previous statistical results [*Liou et al.*, 2001]. The solar wind flow speed was low, ~300 km s^{-1}, and the dynamic pressure was ~2–3 nPa with small amplitude fluctuations.

2.2. THEMIS ASI Observations

[12] Figure 2 shows selected auroral images taken by the THEMIS ASIs at Fort Yukon (FYKN) and Whitehorse (WHIT) before, at, and after the onset in geomagnetic (white dotted lines) and geographic (green dotted lines) coordinates. Enlarged plots focusing on the center of the FYKN ASI are shown on the right. The THEMIS ASIs are white light CCD cameras with a temporal resolution of 3 s and a spatial resolution of ~1 km at magnetic zenith. Details of the THEMIS ASI are described by *Mende et al.* [2008]. Near the edge where the two imagers' FOVs overlap, the same ray aurora present different morphology due to projection effects. Locations of the footprints of Reimei (red asterisks), beams of PFISR (plus signs), Geotail (green triangle) and three ground magnetometers at Fort Yukon, Eagle, and Poker Flat (red diamonds) are also denoted. The FOVs of the Reimei camera mapped to 110 km altitude for the 670.0 nm wavelength at time 1119:46.999 UT and 1119:51.061 UT are shown by the blue squares in the images taken at 1119:45 and 1119:51 UT (see section 2.3 for the Reimei image observations). The time difference is because of the different time cadences (3 s and 120 ms) of THEMIS ASI and Reimei MAC, respectively. Geotail observations are shown in section 2.5. Movies S1–S2 of the FYKN and WHIT ASI observations from 1100 to 1200 UT with a 3 s cadence and enlarged FYKN ASI observations from 1116 UT to 1126 UT are provided as auxiliary material.[1]

[13] In the image taken at 1117:00 UT, two east-west oriented arcs can be seen. The luminosity of the brighter, more equatorward arc had started to increase gradually at ~1116:18 UT, and the brightening rapidly propagated westward along the arc from the east at ~1117:00 UT. At the same time, the arc started to develop wave-like structures. However, this luminosity enhancement lasted for only one minute, as shown in the movie. At ~1118:51 UT, it brightened from the east again, and the brightening drifted westward and formed wave-like structures (see enlarged images taken at 1119:27 and 1119:45 UT). Similar wave-like structures have been associated with ray auroras [*Sakaguchi et al.*, 2009]. The spatial wavelength of these structures was ~1.5° geomagnetic longitude (mlon), within the typical range reported by *Liang et al.* [2008] and such perturbations can propagate either westward or eastward [*Donovan et al.*, 2006, 2008; *Liang et al.*, 2008; *Henderson*, 2009; *Uritsky et al.*, 2009]. While the second brightening of the most equatorward arc and formation of the wave-like structures at 1118:51 UT could be identified as the substorm onset based on the traditional definition by *Akasofu* [1964], our observations show that it did not break up, i.e., initiate poleward expansion, and thus we do not define this as the onset.

[14] A new arc poleward of the most equatorward arc became discernible at ~1119:06 UT, as denoted by an orange arrow in the image at 1119:27 UT. We refer to this arc as the poleward arc in the rest of the text. It slowly brightened and then extended southwestward. At 1119:42 UT, its equatorward end brightened suddenly and from 1119:45 UT it rapidly expanded azimuthally and poleward, denoted by the blue arrow in the second enlarged image. We consider this phenomenon as the auroral breakup, and thus the onset time of this auroral breakup is determined to be 1119:42 UT, consistent with the onset time determined based on ground magnetometer data (described below). Later, the breakup arc engulfed the wavy arc and they evolved together, and it became impossible to distinguish them. A clockwise auroral spiral, the typical form of the WTS, later developed in the center of the FYKN ASI at ~1122:00 UT and slowly drifted westward.

[15] Figure 3a shows a keogram of the FYKN ASI and magnetic perturbations recorded by the three magnetometers from 1030 UT to 1200 UT, and Figure 3b shows Pi1 pulsations (2–40s) calculated from them from 1100 UT to 1150 UT. In both panels, the vertical solid line indicates the substorm onset time and two vertical dashed lines indicate the initiation times of the two auroral brightenings at the most equatorward arc, as described above. In Figure 3a, there were two arcs during the growth phase, identified by two arrows, and both moved gradually to lower latitude. The poleward arc was fainter than the equatorward one. After onset, aurora rapidly expanded poleward and lasted for at least 40 min, which indicates that this is a substorm not a pseudobreakup. As can be seen, the first auroral brightening described above occurred at the most equatorward arc a couple of minutes before the onset and lasted for about 1–2 min. This aurora brightening was also associated with a short-lived Pi1 perturbation, most clearly by the EAGL magnetometer, and a very small negative perturbation in the magnetic H component before the onset.

2.3. Reimei Observations

[16] Reimei is the first satellite with ability to image fine-scale (~1 km) structures of auroral arcs and simultaneously measure the precipitating particles responsible for the auroral features [*Saito et al.*, 2001]. Reimei is orbiting around the Earth at an altitude of ~640 km in a Sun-synchronous orbit of 98.6° inclination crossing the equator at 0.6 and 12.6 MLT [*Sakanoi et al.*, 2003; *Obuchi et al.*, 2008]. Reimei is equipped with a three-channel monochromatic auroral imaging camera (MAC) and an electron/ion energy analyzer (EISA). MAC can measure emissions with 120 ms cadence at wavelengths of 427.8 (N_2^+ 1N), 557.7 (OI), and 670.0 (N_2 1P) nm, and has a FOV that projects to 70 × 70 km at 110 km altitude with spatial resolution of 1.2 × 1.2 km^2 [*Sakanoi et al.*, 2003; *Obuchi et al.*, 2008]. EISA can measure particles with energy ranging from 10 eV/q to 12 keV/q with a temporal resolution of 20/40 ms for 16/32 energy steps and a full pitch angle coverage [*Asamura et al.*, 2003].

[17] On this day, coincidently, Reimei crossed the onset region just at the time when the rapid expansion commenced. To the best of our knowledge, it captured the first high temporal and spatial resolution satellite images of a portion of the breakup arc and the wave-like structures, as well as the corresponding precipitating electrons for the latter. The FYKN and WHIT ASIs provide mesoscale auroral images with a 3 s cadence as described in section 2.2, and together with the Reimei auroral observations, they enable us to put the fine-scale features into the context of the larger-scale auroral substorm dynamics.

[18] Figure 4a presents Reimei MAC images of the two arcs taken at three wavelengths in geographic coordinates at 1119:46.999 UT (first row) and 1119:51.061 UT (second

[1] Auxiliary materials are available in the HTML. doi:10.1029/2010JA015520.

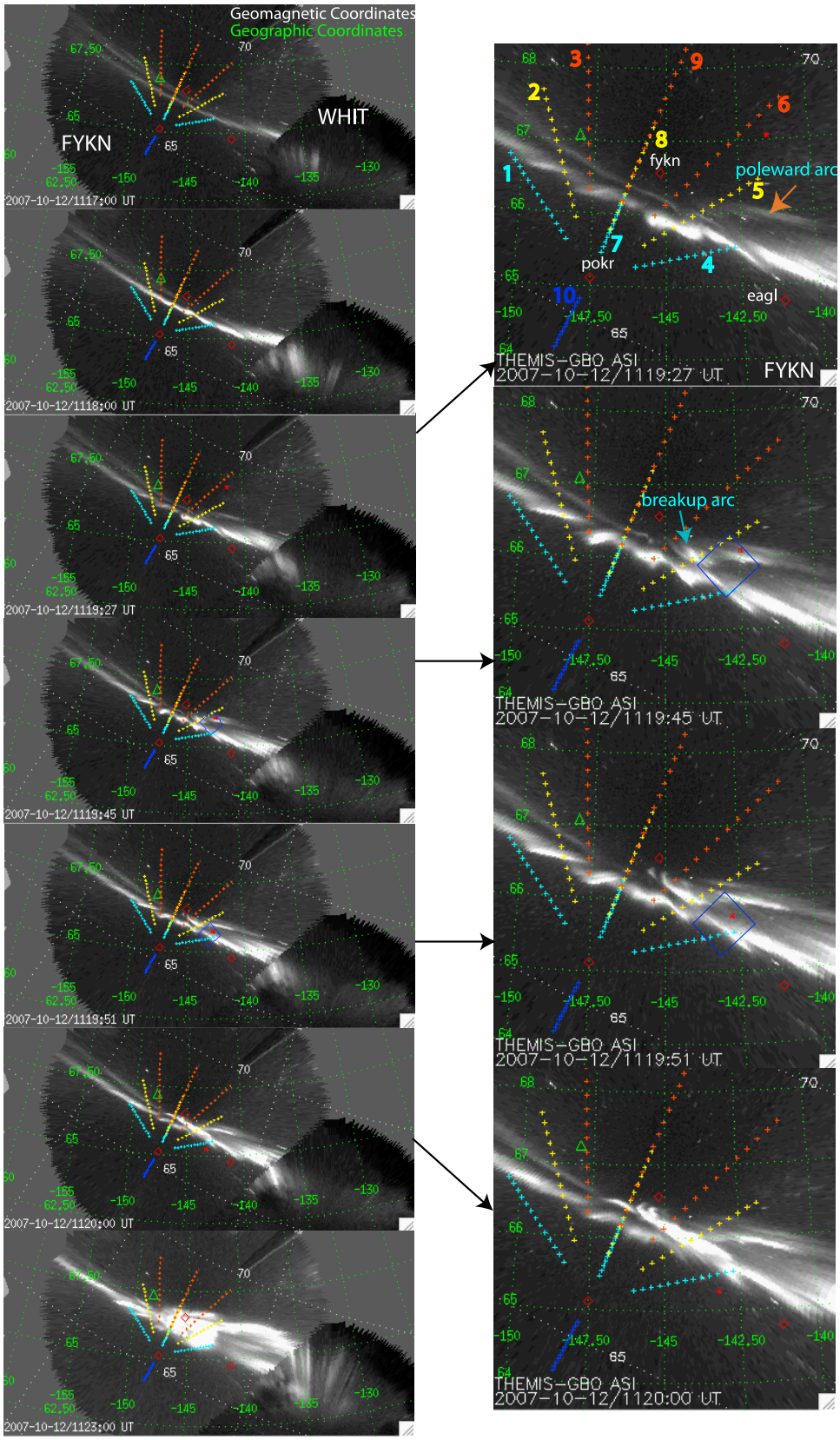
Geomagnetic Coordinates
Geographic Coordinates
FYKN
WHIT
2007-10-12/1117:00 UT
2007-10-12/1118:00 UT
2007-10-12/1119:27 UT
2007-10-12/1119:45 UT
2007-10-12/1119:51 UT
2007-10-12/1120:00 UT
2007-10-12/1123:00 UT
fykn
pokr
eagl
poleward arc
breakup arc
THEMIS-GBO ASI
2007-10-12/1119:27 UT
FYKN
THEMIS-GBO ASI
2007-10-12/1119:45 UT
THEMIS-GBO ASI
2007-10-12/1119:51 UT
THEMIS-GBO ASI
2007-10-12/1120:00 UT

Figure 2

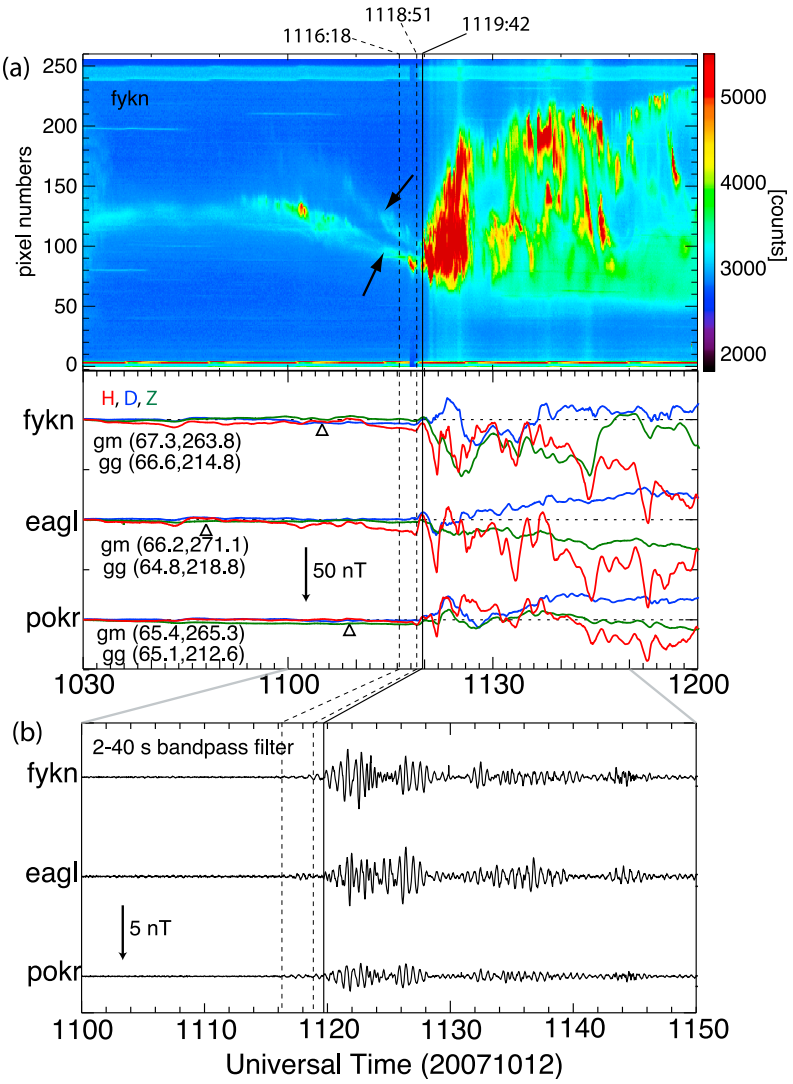

Figure 3. (a) Auroral keogram from the center of FYKN ASI, and the *H*, *D*, and *Z* components of magnetic perturbations recorded by the three magnetometers from 1030 to 1200 UT. Triangles indicate the magnetic midnights in UT. Locations of the magnetometers in geomagnetic and geographic coordinates are also labeled. (b) Pi1 pulsations (2–40 s) calculated from the 1 s temporal resolution magnetometer data. The vertical solid line indicates the substorm onset time at 1119:42 UT, determined by the THEMIS ASI observations. The two vertical dashed lines indicate the initiation times of the two auroral brightenings at the most equatorward arc at 1116:18 and 1118:51 UT.

row). Movie S3 containing continuous observations from MAC between 1119:14 and 1120:14 UT with a ~120 ms time resolution is available as auxiliary material. White diamonds in the images indicate the footprint of the Reimei satellite based on the IGRF geomagnetic field model [*Obuchi et al.*, 2008]. The FOV of the two images taken in the wavelength of 670.0 nm at the corresponding time are shown in the images taken at 1119:45 and 1119:51 UT in Figure 2. Figure 4b shows the electron and ion energy spectra at three different pitch angle ranges measured by the Reimei EISA from 1119:35 UT to 1120:10 UT. The particle energy spectra over the entire auroral oval were measured

Figure 2. (left) Selected auroral images taken by the THEMIS FYKN and WHIT ASIs and (right) enlarged images near the center of the FYKN ASI in geographic coordinates (green). Geomagnetic coordinates (white) are also shown for reference. The footprints of Reimei (red asterisk) and Geotail (green triangle) at the time when the image was taken, beams of PFISR (plus signs), and ground magnetometers (red diamonds) are denoted. Beam numbers of PFISR are shown on the top right image. Each plus sign of the PFISR beam represents the location of data point from the long pulse radar measurement, which has a range resolution of 72 km. Blue squares in images taken at 1119:45 UT and 1119:51 UT indicate the FOV of Reimei MAC at 1119:46.999 UT and 1119:51.061 UT at 110 km altitude in the wavelength of 630.0 nm (observations of Reimei MAC are shown in Figure 4).

within ~23 s after 1119:41 UT at ~0.6 MLT, and provide information about the characteristics of the precipitating electrons causing the aurora fine-scale structures and indirectly about the magnetospheric source region where they originate. The whole auroral oval, bounded by the two magenta vertical lines in Figure 4, was very narrow, only ~1.5° geomagnetic latitude (mlat), consistent with the image shown in Figure 2.

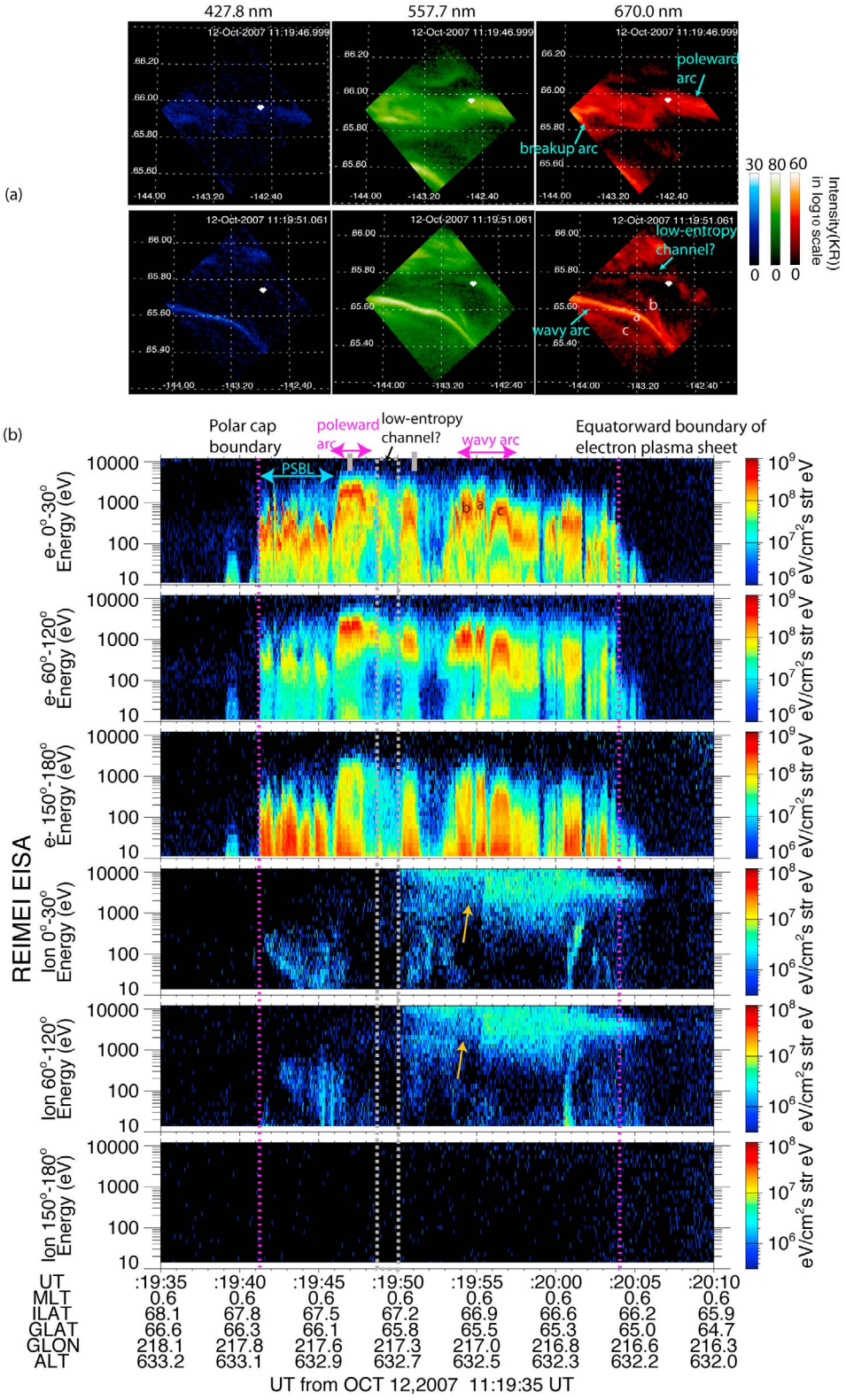

Figure 4

[19] As Reimei moved from higher to lower latitudes, it first encountered the polar cap boundary, which is clearly marked by the sudden appearance of precipitating electrons with energies up to ~1 keV in the 0° to 30° pitch angle bin. These electrons were distributed in a broad energy range and peaked in the downward direction. Together with the detected velocity-dispersed low-energy ions, this region immediately equatorward of the separatrix should map to the plasma sheet boundary layer (PSBL), as suggested by *Fukunishi et al.* [1993]. These broadband electrons were associated with very faint auroral emission, as can be seen in Figure 4a (top) above 66.0° geographic latitude (glat) and in the movie.

[20] After passing the PSBL, Reimei crossed the poleward arc, denoted by the orange arrow in Figure 2, from ~1119:46 to ~1119:48 UT (first magenta horizontal arrow in Figure 4b). Based on the image in the first row of Figure 4a, the arc width was on the order of 20 km. The FOV of Reimei MAC at 1119:46.999 UT, i.e., the time when the auroral images in Figure 4a (top) were taken, is shown as a blue square in the second image of Figure 2 (right). Comparison between the two images enables us to put the Reimei observations into a larger-scale auroral context. The brightest portion of the arc near the western edge corresponds to part of the breakup arc shown in Figure 2, while the aurora near the eastern edge corresponds to part of the poleward arc. As shown in the movie, there was rapid shear motion on the two sides of the poleward arc with eastward in geographic coordinates (northeastward in geomagnetic coordinates) drifting aurora on the poleward side and westward (southwestward) drifting aurora on the equatorward side. The shear motion in the 557.7 nm images is not as obvious as that in 670.0 nm, because the 557.7 nm (OI) emission has a much longer lifetime than the N_2 1P emission near 670.0 nm emission [*Obuchi et al.*, 2008]. Although Reimei cannot measure electric fields, under the E × B motion assumption, the shear motion orientation suggests southward electric fields on the poleward side and northward electric fields on the equatorward side, and therefore converging electric fields, consistent with the aurora brightening and thus upward FACs in the center.

[21] As shown in Figure 4b, the poleward arc was associated with monoenergetic electron precipitation with an energy peak at ~2 keV at ~67.4° mlat, and a relatively isotropic pitch angle distribution except in the upward direction, consistent with the characteristics of an inverted V arc. Broadband electrons can also be seen near the poleward shoulder of this inverted V arc. Broadband electrons are usually associated with Alfvén waves [e.g., *Chaston et al.*, 2000; *Mende et al.*, 2003]. Morphologically, this poleward arc should be mapped to the tailward part of the plasma sheet, based on results of *Fukunishi et al.* [1993]. Ion energy spectra between 1119:46.5 and 1119:50 UT show a lack of precipitating ions within the energy range of the detector. The lack of ions within the poleward arc region, i.e., between 1119:46.5 and 1119:48 UT, is likely due to the presence of the potential drop suggested by the monoenergetic electron precipitation. This potential drop can decelerate the precipitating ions and even reflect those with energies below the potential drop [*Coumans et al.*, 2004]. However, the region just equatorward of the poleward arc, highlighted by a gray box in Figure 4b, also shows reduced precipitating ions. Assuming strong pitch angle diffusion in the plasma sheet, reduced ion precipitation in the region with an absence of a potential drop implies a possibility that the source region in the plasma sheet had a reduced number of available ions, which is one of the features of a low-entropy flow channel. The corresponding region is also denoted Figure 4a (bottom right).

[22] After passing a weak arc structure at ~1119:50 UT, Reimei crossed the wave-like structures from ~1119:54 to ~1119:57 UT (second magenta horizontal arrow in Figure 4b). The weak arc was associated with an inverted V structure detected at ~1119:50 UT and its optical signature can be seen in Figure 4a (bottom) near the footprint of the Reimei satellite at ~65.8° geographic latitude. It is clearer in the 670 nm wavelength than it in the other two wavelengths. In the center of these three images, there is a bright, thin, and highly structured arc, labeled "a." The arc width was only ~4 km and unlike the poleward and breakup arcs, this arc was very stable during the ~10 s when it was within the MAC FOV. As shown in Figure 4b, this thin arc was also associated with inverted V electron precipitation with an energy flux peak at ~1 keV. There were two more inverted V structures adjacent to this one and associated with auroral arcs with much weaker emission, labeled "b" and "c" (Figure 4a). In contrast to the poleward arc, these arcs were fully embedded in energetic ion precipitation, similar to the results by *Samson et al.* [1992]. A reduction in the ion fluxes collocated with the arcs a and b detected at ~1119:54–1119:55 UT, identified by two arrows in the ion energy spectra, is also likely due to the presence of a potential drop.

[23] Although Reimei did not measure the particle precipitation associated with the breakup arc portion, which was further to the west, the magnetospheric source region where the corresponding precipitating electrons originate can be approximately inferred from the ion energy spectra with the assumption of geomagnetic longitudinal homogeneity within a degree. The breakup occurred just poleward of the energetic ion precipitation, consistent with results presented by *Deehr and Lummerzheim* [2001] and *Kadokura et al.*

Figure 4. (a) Selected auroral images taken by the Reimei MAC instrument at three wavelengths in geographic coordinates. Images in the first row were taken at 1119:46.999 UT and those in the second row were taken at 1119:51.061 UT and the time is shown at the top of each image. White diamonds denote the footprint of the Reimei satellite based on the IGRF magnetic field model. (b) Electron and ion energy spectra at three different pitch angle ranges measured by Reimei EISA. The total time span is 35 s from 1119:35 UT. The horizontal axis is labeled with UT, magnetic local time (MLT), invariant latitude (ILAT), geographic latitude of the satellite footprint (GLAT), geographic longitude of the satellite footprint (GLON), and altitude of the satellite (ALT). Two horizontal magenta arrows at the top of Figure 4b indicate the period when Reimei passed the poleward arc and the most equatorward arc observed in Figure 2. Two gray bars at the top of Figure 4b denote the corresponding time when the Reimei MAC images shown in Figure 4a were taken.

[2002]. The arc expanded azimuthally initially just poleward of the poleward edge of the wave-like structures and also along the poleward boundary of the ion precipitation under the assumption that the ion precipitation boundary is located roughly at a fixed geomagnetic latitude. This observation is similar to *Oguti* [1973], in which meridian scanning photometer and ASI observations were used.

2.4. PFISR Observations

[24] Figure 5 shows time series of convection flows (Figure 5a) and electron densities (Figures 5b–5d) measured by three central northward looking beams of PFISR from 1045 to 1200 UT. Details about the convection flow calculation are described by *Heinselman and Nicolls* [2008]. The magenta and gray vertical lines indicate the substorm onset time determined by the THEMIS ASI observations at 1119:42 UT and the start time of a rapid equatorward motion of the auroral oval inferred from the electron density profiles at ~1108 UT, respectively. This sudden equatorward motion might be related with the weak southward turning in Figure 1 at about the same time.

[25] At the substorm onset, the equatorward and poleward boundaries of the auroral oval were located at ~66.2° (Figure 5d) and 67.3° mlat (Figure 5b), respectively. Due to the limited radar FOV, the poleward boundary at 67.3° mlat could have been underestimated and could have extended to the higher latitude of ~67.7° mlat as measured by Reimei.

[26] As seen in Figure 5a, the Harang reversal formed during the growth phase as suggested by the flow reversal near the top Figure 5, starting at 1115 UT. The Harang reversal is a feature of the Region 2 current system and an indication of buildup of the dawn-dusk pressure asymmetry in the near-Earth magnetosphere [*Erickson et al.*, 1991]. Based on the RCM simulation results shown by *Gkioulidou et al.* [2009], formation of the Harang reversal in the ionosphere is a manifestation of strengthening of the partial ring current and Region 2 current system during the growth phase.

[27] The wave-like structures located at ~66.8° mlat before onset were embedded within westward flows, while the breakup arc located at ~67.2° mlat was at the center of the Harang reversal, consistent with previous observations of *Zou et al.* [2009a, 2009b]. Because of the limited FOV of PFISR, large-scale 2-D convection flows are not available. The westward flows near the equatorward portion of the PFISR FOV increased after the onset time and reached their peak when the WTS was located near the center of PFISR FOV at ~1122–1124 UT. The *E* region electron density enhancement related with the WTS can be seen in Figure 5b. The flow and density relationship is consistent with the results of *Zou et al.* [2009b], who suggested that this may be an indication of local current closure between the Region 2 FAC equatorward of the onset arc and the substorm current system.

[28] In addition, the altitude extension of the wave-like structures shown in Figure 2 can also be estimated by the density profile. As shown in Figures 5d and 5c, they extended up to ~350 km at ~66.76° mlat and ~270 km at 67° mlat, roughly corresponding to the poleward and equatorward limit of the wave-like structures. Such tall density enhancements correspond to precipitating electrons with broad energy range and are consistent with rayed aurora observations in the FOV of the WHIT ASI.

2.5. Geotail Observations

[29] Figure 6 shows, from 1000 to 1200 UT, the ion moments with 12 s temporal resolution from the Geotail low-energy particle (LEP) instrument [*Mukai et al.*, 1994] and the magnetic field observations with 3 s temporal resolution from the magnetic field experiment (MGF) instrument [*Kokubun et al.*, 1994], respectively. The Geotail spacecraft locations are shown in GSM coordinates and its footprint has been mapped into the ionosphere in Figure 2 using the *Tsyganenko 96* model [*Tsyganenko*, 1995] and the propagated solar wind and IMF as input. As can be seen in Figure 2, near the substorm onset time, the Geotail spacecraft was located slightly poleward of the faint poleward arc and about 0.3 MLT to the west of substorm onset.

[30] The ion β ($= NKT/(B^2/2\mu_0)$) [*Miyashita et al.*, 2000] is shown in the bottom panel, which is the ratio between ion thermal pressure and magnetic pressure. The two horizontal dashed lines give values of β that roughly mark the transition between the plasma sheet, the PSBL, and the lobe, based on the formula used by *Miyashita et al.* [2000]. The gray vertical line indicates the time when the Geotail spacecraft started to cross from the northern PSBL to the northern lobe at 1108:22 UT, as indicated by the substantial decrease of the ion β, ion density and ion temperature. The crossing took about 6–7 min and during this period, the Geotail spacecraft was essentially stationary and only moved from (−11.06, 0.07, 0.26) R_E to (−11.00, −0.05, 0.38) R_E in GSM coordinates. The total pressure (blue line in the second bottom panel) continued increasing during and after this crossing. The initiation time of the crossing is approximately the same as that of the equatorward shift of the auroral oval inferred from the electron density measurement of PFISR described in section 2.4. These two observations together suggest that the plasma sheet became thinner as the lobe magnetic flux increased and the magnetic field became more stretched. During the crossing, the plasma flow velocity changed from mainly earthward to briefly tailward and then to weakly earthward again.

[31] The magenta vertical line marks the substorm onset time at 1119:42 UT, determined by the THEMIS ASI observation. At this time, the total pressure slightly decreased and the northward B*z* slightly increased, which together suggest dipolarization. Since the spacecraft was located in the lobe, any flows accompanied this dipolarization could not be measured. At ~1127 UT, the Geotail spacecraft moved from the northern lobe back to the PSBL and later into the plasma sheet, inferred from the ion β variation, which indicates plasma sheet expansion. The auroral image movie shows that the WTS swept the footprint of Geotail roughly at this time. Three bursts of fast flow and dipolarization were detected by Geotail later during the expansion phase, when it was located mainly in the plasma sheet.

3. Discussion

[32] It is frequently observed that the breakup arc is the most equatorward one [*Akasofu*, 1964; *Lyons et al.*, 2002]. It usually initiates from wave-like auroral enhancements, or auroral beads, and they subsequently develop into vortical structures and lead to breakup [e.g., *Elphinstone et al.*, 1995; *Donovan et al.*, 2006, 2008; *Liang et al.*, 2008; *Henderson*, 2009]. These wave-like auroral enhancements have been

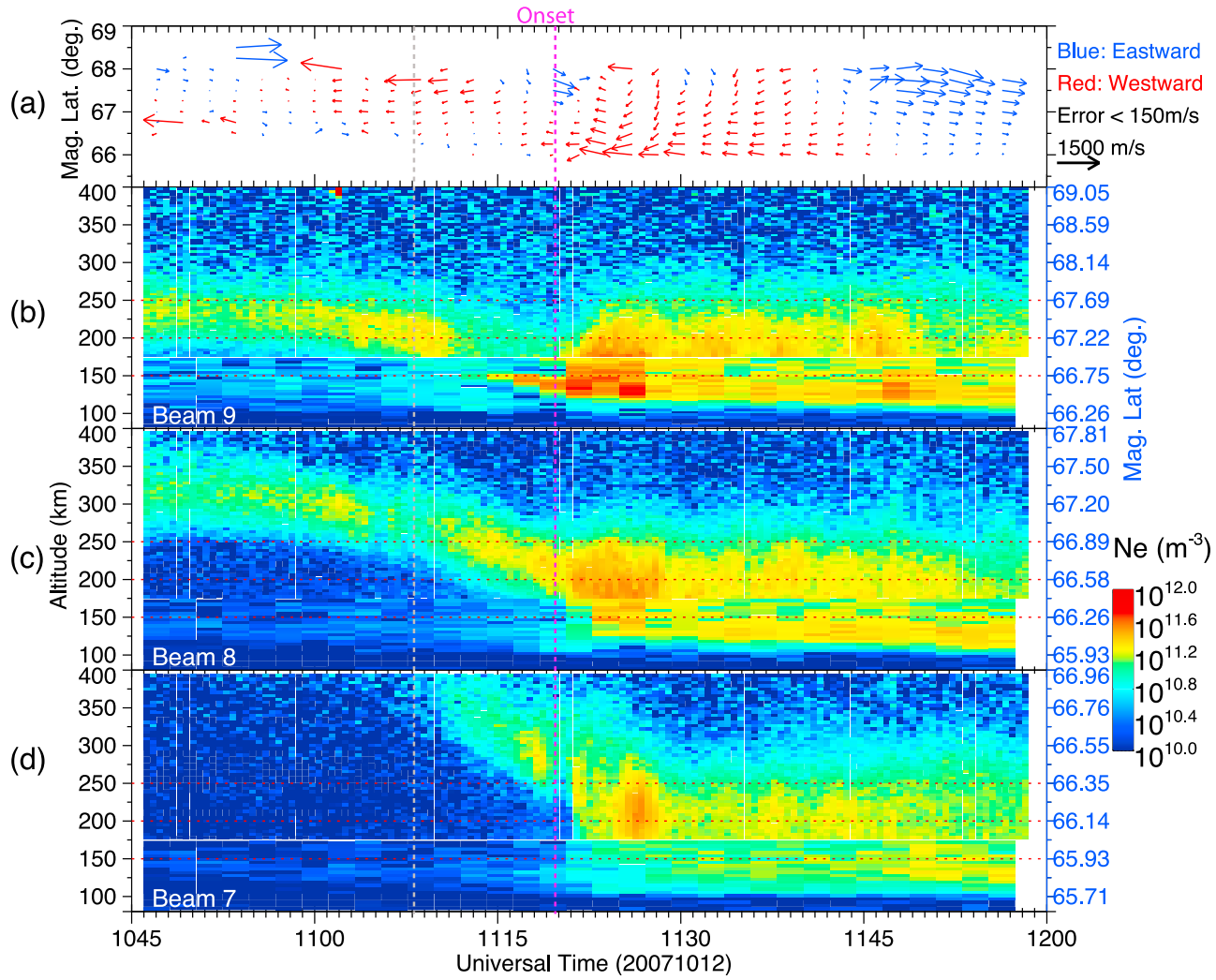

Figure 5. (a) Nightside convection flows measured by PFISR on 12 October 2007 are shown as a function of magnetic latitude and UT; data are plotted only if the measurement uncertainty is less than 150 m/s. Flows with eastward component are blue, and those with westward component are red. (b–d) Raw electron densities with no correction for T_e/T_i or Debye length effects measured by three central northward looking beams are shown as a function of UT. Altitude (magnetic latitude) is indicated on the left (right) Y ordinate. The electron density below 175 km is from the alternating code pulse measurement, while that above 175 km is from the long pulse measurement. The magenta and gray vertical lines indicate the substorm onset time determined by the THEMIS ASI observations at 1119:42 UT and the start time of a rapid equatorward motion of the auroral oval inferred from the electron density profiles at ~1108 UT, respectively.

suggested to be a manifestation of the existence of plasma instability waves at the near-Earth plasma sheet [*Elphinstone et al.*, 1995; *Donovan et al.*, 2006; *Liang et al.*, 2008; *Henderson*, 2009], such as ballooning instability [*Liang et al.*, 2008; *Henderson*, 2009]. The ballooning instability [*Roux et al.*, 1991; *Pu et al.*, 1997; *Cheng and Lui*, 1998; *Cheng*, 2004] becomes more unstable under a tail-like magnetic field configuration [*Miura*, 2001, and references therein]. Indeed in the present study, signatures of plasma sheet thinning were observed by both Geotail and PFISR ~8 min prior to the wave-like auroral enhancement. *Saito et al.* [2008] found solid ballooning mode signatures 1 to 3 min prior to the auroral breakup in 4 out of 6 substorm events using observations from Geotail. During these four events, Geotail was located in the equatorial plane with radial distance ranging from ~–10 to ~–13 R_E. The wave-like auroral enhancement in the present case initiated ~3 and 1 min before the breakup, consistent with the timing found by *Saito et al.* [2008]. Unfortunately, in the present case, the Geotail spacecraft was located in the lobe and thus cannot be used to further analyze the type of instability.

[33] The wave-like auroral enhancement thus likely represents the ballooning instability in the near-Earth plasma sheet. However, in this example, it did not develop further or expand spatially, and was thus not the breakup arc. Instead, the auroral breakup occurred just poleward of the wave-like structures, which is different from a common onset sequence [*Donovan et al.*, 2006, 2008; *Liang et al.*,

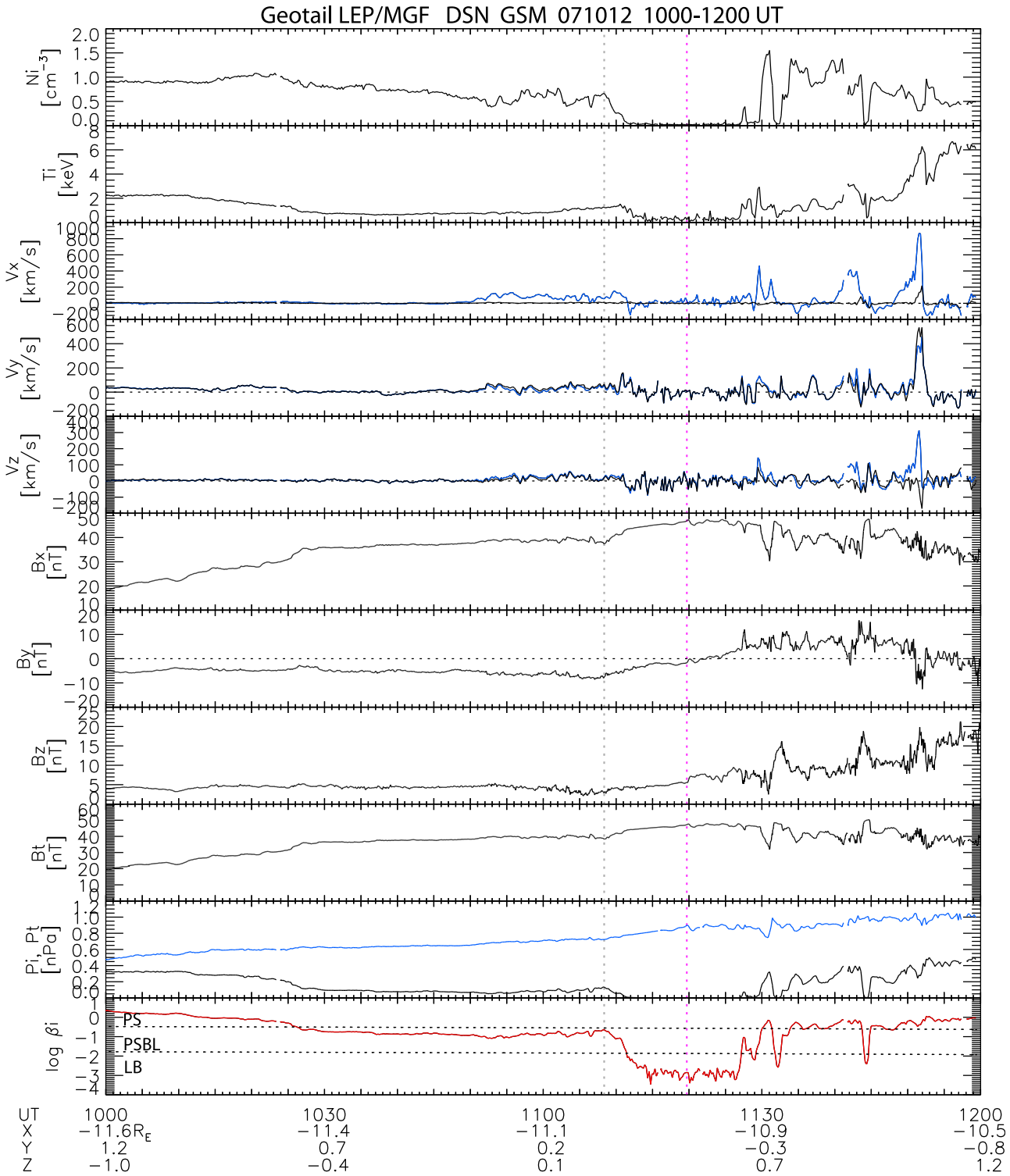

Figure 6. Geotail LEP and MGF observations in GSM coordinates from 1000 to 1200 UT. (top to bottom) The ion number density, the ion temperature, the three components of the ion velocity (blue lines) and the ion velocity perpendicular to the magnetic field (black lines), the three components of the magnetic field, the total magnetic field, the total (blue line) and ion (black line) pressures, and the ion beta are shown. The gray vertical line indicates the time when the Geotail spacecraft started to cross from the northern PSBL to the northern lobe at 1108:22 UT. The magenta vertical line indicates the substorm onset time at 1119:42 UT determined by the THEMIS ASI observations.

2008; *Henderson*, 2009]. That this distinction has not been reported previously, could be because it occurs rarely or due to the limitation of imaging instrumentation. In order to resolve thin auroral arcs and their rapid variations, optical instruments with a temporal resolution of a couple of seconds and a spatial resolution of ~1 km, such as the THEMIS ASI, are required. Lower temporal and spatial resolutions than these could only capture the merged and expanded arc as a whole. In addition, even given spatial resolution as high as THEMIS ASI, the thin arcs need to be close enough to the magnetic zenith to be distinguished. A statistical study of the THEMIS ASI data is necessary to determine the occurrence rate of such phenomena. However, the presence of the wave-like auroral enhancement before the breakup may imply an important precondition of the near-Earth plasma sheet for the subsequent onset.

[34] The poleward arc occurred just adjacent to the PSBL and is thus probably a PBI. A PBI being usually defined as intensification of nightside discrete aurora at or near the polar cap boundary [*Lyons et al.*, 1999; *Zesta et al.*, 2002]. It is primarily studied using meridian scanning photometer data and UV images [*Zesta et al.*, 2002, 2006, and references therein]. Based on *Fukunishi et al.* [1993, Figure 7], the inverted V particle precipitation responsible for generating the highest-latitude discrete aurora is just adjacent to the PSBL. Therefore, we identify the poleward arc here as a PBI. In the present case, the breakup arc appears to have occurred along the southwestward extension of this arc. Their relationship is analogous to that of the PBI to the auroral streamer [*Zesta et al.*, 2000]. The auroral streamer is believed to be the ionospheric manifestation of flow bursts [*Angelopoulos et al.*, 1992, 1994] in the plasma sheet [e.g., *Zesta et al.*, 2000; *Sergeev et al.*, 2000], which are associated with reconnection in the magnetotail. In the present case, we suggest the poleward arc brightening implies a reconnection process in the magnetotail, although we cannot determine solely based on ionospheric observations whether the reconnection is at the distant X line or a near Earth one. The orientation of the auroral streamer could have been affected by the polarity of the prevailing IMF *By* [*Zesta et al.*, 2006; *Nakamura et al.*, 2001; *Sergeev*, 2002; *Henderson et al.*, 2001]. In our case, the IMF *By* was strongly negative for about 50 min before the onset and the arc was tilted clockwise, similar to the example shown by *Nakamura et al.* [2001]. Within the frame of a thick auroral oval or double oval configuration, the auroral streamer is easier to identify. In our case, because the oval was very thin, the PBI and its extension, i.e., the breakup arc, were nearly east-west aligned and their latitude coverage was rather limited. Without the concurrent Reimei particle and PFISR electron density measurements, we would not be able to identify their nature and possible magnetospheric source region.

[35] In the present event, the rapid southwestward motion of the aurora on the equatorward side of the PBI is probably associated with fast southwestward flows. Since the ion precipitation is also significantly reduced in this region, there is likely a low-entropy flow channel just on the equatorward side of the arc, lending some support to the scenario proposed by *Nishimura et al.* [2010]. As shown in the auroral image taken at 1119:45 UT in Figure 2, this flow channel is expected to be mapped to the dark region between the poleward arc and the wave-like auroral enhancement. Most of the events examined by *Nishimura et al.* [2010] occur within a relatively well-defined wide auroral oval and the auroral streamers are then easily identified. For the present event, the relation between the poleward arc and the breakup arc would be analogous to the auroral streamer and the breakup arc shown by *Nishimura et al.* [2010]. However, because the oval is so thin in this case and the IMF By has been strongly negative for a long period, the poleward arc is nearly in the east-west direction instead of the more common north-south direction. This could offer a possible explanation for why motion of an east-west arc is observed before the breakup occasionally in their database. However, there is no direct measurement of the flows at this region in this case. Future conjugate studies are required to uncover the ionospheric signature of the low-entropy flow channel and its role in substorm triggering.

[36] Much effort has been devoted to investigate whether there might be a causal link between the near-Earth ballooning instability and near-Earth reconnection [e.g., *Voronkov et al.*, 2000; *Zhu et al.*, 2007]. As shown by numerical simulation of *Zhu et al.* [2007], the growth of the ballooning instability could lead to enhanced thinning of the current sheet, which could increase the possibility of reconnection. In this substorm event, the auroral oval was extremely thin and its poleward boundary was ~67.7° mlat, which suggests the possibility that the distant reconnection site may be less far downtail than usual, so that the near-Earth process might affect the distant reconnection as well. Further evaluation of any possible relation between the near-Earth instability and reconnection, either the near-Earth or distant tail one, is beyond our current analysis and requires in situ observations as well.

4. Summary and Conclusions

[37] In this paper, we reported a fortuitous substorm event that occurred at ~1119 UT on 12 October 2007, of which observations were obtained simultaneously from a polar-orbiting satellite, ground-based imager, magnetometers and radar. This was an isolated substorm within a very thin auroral oval. However, rich auroral fine structures were observed. The MAC cameras onboard Reimei captured a portion of the breakup arc, and wave-like structures further equatorward. To the best of our knowledge, it is the first high spatial and temporal resolution satellite image of those auroral forms. The present observations include many fundamental elements of substorms and the order of their occurrence suggests important possible causal relations between them. Time sequence of events observed and their possible underlying magnetospheric sources are listed in Table 1. Major observations and their implications described in the text are listed below:

[38] 1. About 11 min before the substorm onset, the Geotail spacecraft experienced a crossing from the northern PSBL to the northern lobe. Coincident with this crossing, the auroral oval observed from ASIs and inferred from the electron density observations from PFISR shifted equatorward. These observations together suggest that the plasma sheet became thinner.

[39] 2. Wave-like auroral enhancements appeared twice at the most equatorward preexisting auroral arc about three minutes and one minute before the rapid auroral expansion. Unlike the frequently observed sequences, neither

Table 1. Time Sequence of Observations for 12 October 2007 Substorm

UT	Observation	Interpretation
~1108	Auroral oval quickly moves equatorward; Geotail moves from the northern plasma sheet boundary layer to the northern lobe;	Plasma sheet thinning
1116:18	First luminosity increase at the most equatorward arc and the brightening propagates westward; Formation of wave-like structures; The brightening lasts for only one minute;	Near-Earth instability
1118:51	Second luminosity increase at the most equatorward arc and the brightening propagates westward; Formation of wave-like structures;	Near-Earth instability
1119:06	Initiation of the poleward arc and its southwestward extension	Magnetic reconnection and earthward moving low-entropy flow channel
1119:42	Initiation of auroral poleward expansion[a]	Near-Earth instability

[a]This phenomenon is defined as onset.

enhancement developed into auroral breakup. The part of the most equatorward arc captured by Reimei was associated with three fine inverted V structures, fully embedded in energetic ion precipitation, and was located in westward convection flows. These wave-like structures are likely associated with ballooning instability.

[40] 3. A new arc, poleward of the most equatorward preexisting auroral arc and adjacent to the PSBL, initiated about 40 s before the auroral expansion and after the wave-like auroral enhancement and was likely a PBI. This arc was associated with inverted V electron precipitation in a region of absence of ion precipitation, which extended further equatorward of the arc. Rapid shear motion in the aurora was observed on both sides of the arc.

[41] 4. This poleward arc extended southwestward and led to the auroral breakup. The breakup arc was located poleward of and separated from the most equatorward arc. Under the assumption that the proton precipitation is longitudinally homogeneous over one degree in geographic longitude, the breakup arc was also located within the region of absence of ion precipitation just poleward of the energetic ion precipitation. PFISR observation indicates that the breakup arc was also located within the center of the Harang reversal. There is evidence of rapid southwestward ionospheric flows equatorward of the poleward arc and the breakup arc based on the high temporal auroral observations from Reimei MAC. These rapid southwestward flows were within a region of absence of energetic ion precipitation and might be the ionospheric manifestation of a low-entropy flow channel. Future conjugate study is needed to further test this possibility.

[42] 5. Observations from Reimei MAC revealed a distinct difference in auroral morphology between the breakup arc and the wave-like auroral enhancement. The former was structureless and very dynamic associated with rapid shear motion within the arc, while the latter was very stable for ~10 s when within the MAC FOV.

[43] 6. We would like to draw attention to the fact that in this event the arc that initiated the poleward expansion was not the most equatorward arc with wave-like auroral structures, which brightened earlier, but a southwestward extension of the arc adjacent to the PSBL.

[44] We emphasize that this is only a single event with fortuitous multiple instrument observations. Therefore, whether features of this event are common or rare cannot be determined and need analysis of more events. It would be particularly interesting to determine whether or not the distinction between the most equatorward wavy arc and the breakup arc is common, and whether there is a low-entropy flow channel associated with the breakup arc.

[45] **Acknowledgments.** This research at University of Michigan is partially supported by NASA grant NNX09A162G. This work at UCLA was supported by National Science Foundation grants ATM-0639312 and ATM-0646233 and NASA grant NNX09AI06G. The Poker Flat ISR measurements and analysis is supported under cooperative agreements ATM-0608577 between the U.S. National Science Foundation and SRI International, respectively. THEMIS is funded by NASA contract NAS5–02099. We thank Y. Ebihara for the excellent tool for plotting energy-time spectrograms. Geotail MGF and LEP data were provided by T. Nagai and Y. Saito through DARTS at Institute of Space and Astronautical Science, JAXA in Japan. The magnetometer data are obtained from the Geophysical Institute, University of Alaska, Fairbanks. The provisional AE index is obtained from WDC for geomagnetism, Kyoto. The OMNI data were obtained from the GSFC/SPDF OMNIWeb interface at http://omniweb.gsfc.nasa.gov.

[46] Robert Lysak thanks the reviewers for their assistance in evaluating this paper.

References

Akasofu, S.-I. (1964), The development of the auroral substorm, *Planet. Space Sci.*, *12*, 273, doi:10.1016/0032-0633(64)90151-5.

Akasofu, S.-I., D. S. Kimball, and C.-I. Meng (1965), Dynamics of the aurora, II, Westward traveling surges, *J. Atmos. Terr. Phys.*, *27*, 173, doi:10.1016/0021-9169(65)90114-5.

Akasofu, S.-I., C.-I. Meng, and D. S. Kimball (1966), Dynamics of the aurora, IV, Polar magnetic substorm and westward traveling surges, *J. Atmos. Terr. Phys.*, *28*, 489, doi:10.1016/0021-9169(66)90058-4.

Angelopoulos, V., W. Baumjohann, C. F. Kennel, F. V. Coroniti, M. G. Kivelson, R. Pellat, R. J. Walker, H. Lühr, and G. Paschmann (1992), Bursty bulk flows in the central plasma sheet, *J. Geophys. Res.*, *97*, 4027, doi:10.1029/91JA02701.

Angelopoulos, V., et al. (1994), Statistical characteristics of bursty bulk flow events, *J. Geophys. Res.*, *99*, 21,257, doi:10.1029/94JA01263.

Angelopoulos, V., et al. (2008), Tail reconnection triggering substorm onset, *Science*, *321*, 931, doi:10.1126/science.1160495.

Asamura, K., et al. (2003), Auroral particle instrument onboard the index satellite, *Adv. Space Res.*, *32*, 375, doi:10.1016/S0273-1177(03)90275-4.

Baker, D. N., T. I. Pulkkinen, V. Angelopoulos, W. Baumjohann, and R. L. McPherron (1996), Neutral line model of substorms: Past results and present view, *J. Geophys. Res.*, *101*, 12,975, doi:10.1029/95JA03753.

Chaston, C. C., C. W. Carlson, R. E. Ergun, and J. P. McFadden (2000), Alfven waves, density cavities and electron acceleration observed from the FAST spacecraft, *Phys. Scr.*, *T84*, 64, doi:10.1238/Physica.Topical.084a00064.

Chen, C. X., and R. Wolf (1993), Interpretation of high-speed flows in the plasma sheet, *J. Geophys. Res.*, *98*, 21,409, doi:10.1029/93JA02080.

Cheng, C. Z. (2004), Physics of substorm growth phase, onset, and dipolarization, *Space Sci. Rev.*, *113*, 207, doi:10.1023/B:SPAC.0000042943.59976.0e.

Cheng, C. Z., and A. T. Y. Lui (1998), Kinetic ballooning instability for substorm onset and current disruption observed by AMPTE/CCE, *Geophys. Res. Lett.*, *25*, 4091, doi:10.1029/1998GL900093.

Coumans, V., J.-C. Gérard, B. Hubert, S. B. Mende, and S. W. H. Cowley (2004), Morphology and seasonal variations of global auroral proton precipitation observed by IMAGE-FUV, *J. Geophys. Res.*, *109*, A12205, doi:10.1029/2003JA010348.

Deehr, C., and D. Lummerzheim (2001), Ground-based optical observations of hydrogen emission in the auroral substorm, *J. Geophys. Res.*, *106*, 33, doi:10.1029/2000JA002010.

Donovan, E., S. Mende, B. Jackel, M. Syrjasuo, M. Meurant, I. Voronkov, H. Frey, V. Angelopoulos, and M. Connors (2006), The azimuthal evolution of the substorm expansive phase onset aurora, in *Proceedings of ICS-8*, edited by M. Syrjäsuo and E. Donovan, pp. 55, Univ. of Calgary, Calgary, Alberta, Canada.

Donovan, E., et al. (2008), Simultaneous THEMIS in situ and auroral observations of a small substorm, *Geophys. Res. Lett.*, *35*, L17S18, doi:10.1029/2008GL033794.

Dubyagin, S. V., V. A. Sergeev, C. W. Carlson, S. R. Marple, T. I. Pulkkinen, and A. G. Yahnin (2003), Evidence of near-Earth breakup location, *Geophys. Res. Lett.*, *30*(6), 1282, doi:10.1029/2002GL016569.

Elphinstone, R. D., et al. (1995), Observations in the vicinity of substorm onset: Implications for the substorm process, *J. Geophys. Res.*, *100*, 7937, doi:10.1029/94JA02938.

Erickson, G. M., and R. A. Wolf (1980), Is steady convection possible in the Earth's magnetotail?, *Geophys. Res. Lett.*, *7*, 897, doi:10.1029/GL007i011p00897.

Erickson, G. M., R. W. Spiro, and R. A. Wolf (1991), The physics of the Harang discontinuity, *J. Geophys. Res.*, *96*, 1633, doi:10.1029/90JA02344.

Erickson, G., N. Maynard, W. Burke, G. Wilson, and M. Heinemann (2000), Electromagnetics of substorm onsets in the near geosynchronous plasma sheet, *J. Geophys. Res.*, *105*, 25,265, doi:10.1029/1999JA000424.

Fukunishi, H., Y. Takahashi, T. Nagatsuma, T. Mukai, and S. Machida (1993), Latitudinal structures of nightside field-aligned currents and their relationships to the plasma sheet regions, *J. Geophys. Res.*, *98*, 11,235, doi:10.1029/92JA02031.

Gkioulidou, M., C.-P. Wang, L. R. Lyons, and R. A. Wolf (2009), Formation of the Harang reversal and its dependence on plasma sheet conditions: Rice convection model simulations, *J. Geophys. Res.*, *114*, A07204, doi:10.1029/2008JA013955.

Heinselman, C. J., and M. J. Nicolls (2008), A Bayesian approach to electric field and *E* region neutral wind estimation with the Poker Flat Advanced Modular Incoherent Scatter Radar, *Radio Sci.*, *43*, RS5013, doi:10.1029/2007RS003805.

Henderson, M. G. (2009), Observational evidence for an inside-out substorm onset scenario, *Ann. Geophys.*, *27*, 2129, doi:10.5194/angeo-27-2129-2009.

Henderson, M. G., L. Kepko, H. E. Spence, M. Connors, J. B. Sigwarth, L. A. Frank, H. J. Singer, and K. Yumoto (2001), The evolution of north-south aligned auroral forms into auroral torch structures: The generation of omega bands and Ps6 pulsations via flow bursts, *Eos Trans. AGU*, *82*(47), Fall Meet. Suppl., Abstract SM51B–0809.

Kadokura, A., A.-S. Yukimatu, M. Ejiri, T. Oguti, M. Pinnock, and M. R. Hairston (2002), Detailed analysis of a substorm event on 6 and 7 June 1989: 1. Growth phase evolution of nightside auroral activities and ionospheric convection toward expansion phase onset, *J. Geophys. Res.*, *107*(A12), 1479, doi:10.1029/2001JA009127.

Kepko, L., E. Spanswick, V. Angelopoulos, E. Donovan, J. McFadden, K.-H. Glassmeier, J. Raeder, and H. J. Singer (2009), Equatorward moving auroral signatures of a flow burst observed prior to auroral onset, *Geophys. Res. Lett.*, *36*, L24104, doi:10.1029/2009GL041476.

Kokubun, S., T. Yamamoto, M. H. Acuña, K. Hayashi, K. Shiokawa, and H. Kawano (1994), The GEOTAIL magnetic field experiment, *J. Geomag. Geoelectr.*, *46*(1), 7.

Liang, J., E. F. Donovan, W. W. Liu, B. Jackel, M. Syrjäsuo, S. B. Mende, H. U. Frey, V. Angelopoulos, and M. Connors (2008), Intensification of preexisting auroral arc at substorm expansion phase onset: Wave-like disruption during the first tens of seconds, *Geophys. Res. Lett.*, *35*, L17S19, doi:10.1029/2008GL033666.

Liou, K., P. T. Newell, D. G. Sibeck, C.-I. Meng, M. Brittnacher, and G. Parks (2001), Observation of IMF and seasonal effects in the location of auroral substorm onset, *J. Geophys. Res.*, *106*, 5799, doi:10.1029/2000JA003001.

Lui, A. T. Y. (2004), Potential plasma instabilities for substorm expansion onsets, *Space Sci. Rev.*, *113*, 127, doi:10.1023/B:SPAC.0000042942.00362.4e.

Lui, A. T. Y., R. E. Lopez, B. J. Anderson, K. Takahashi, L. J. Zanetti, R. W. McEntire, T. A. Potemra, D. M. Klumpar, E. M. Greene, and R. Strangeway (1992), Current disruptions in the near-Earth neutral sheet region, *J. Geophys. Res.*, *97*, 1461, doi:10.1029/91JA02401.

Lyons, L. R. (1995), A new theory for magnetospheric substorms, *J. Geophys. Res.*, *100*, 19,069, doi:10.1029/95JA01344.

Lyons, L. R., T. Nagai, G. T. Blanchard, J. C. Samson, T. Yamamoto, T. Mukai, A. Nishida, and S. Kokubun (1999), Association between Geotail plasma flows and auroral poleward boundary intensifications observed by CANOPUS photometers, *J. Geophys. Res.*, *104*, 4485, doi:10.1029/1998JA900140.

Lyons, L. R., I. O. Voronkov, E. F. Donovan, and E. Zesta (2002), Relation of substorm breakup arc to other growth-phase auroral arcs, *J. Geophys. Res.*, *107*(A11), 1390, doi:10.1029/2002JA009317.

Mende, S. B., C. W. Carlson, H. U. Frey, L. M. Peticolas, and N. Østgaard (2003), FAST and IMAGE-FUV observations of a substorm onset, *J. Geophys. Res.*, *108*(A9), 1344, doi:10.1029/2002JA009787.

Mende, S. B., S. E. Harris, H. U. Frey, V. Angelopoulos, C. T. Russell, E. Donovan, B. Jackel, M. Greffen, and L. M. Peticolas (2008), The THEMIS array of ground-based observatories for the study of auroral substorms, *Space Sci. Rev.*, *141*, 357, doi:10.1007/s11214-008-9380-x.

Miura, A. (2001), Ballooning instability as a mechanism of the near-Earth onset of substorms, *Space Sci. Rev.*, *95*, 387, doi:10.1023/A:1005249915285.

Miyashita, Y., S. Machida, T. Mukai, Y. Saito, K. Tsuruda, H. Hayakawa, and P. R. Sutcliffe (2000), A statistical study of variations in the near and mid-distant magnetotail associated with substorm onsets: GEOTAIL observations, *J. Geophys. Res.*, *105*, 15,913, doi:10.1029/1999JA000392.

Mukai, T., S. Machida, Y. Saito, M. Hirahara, T. Terasawa, N. Kaya, T. Obara, M. Ejiri, and A. Nishida (1994), The low energy particle (LEP) experiment onboard the GEOTAIL satellite, *J. Geomag. Geoelectr.*, *46*(8), 669.

Nagai, T., M. Fujimoto, Y. Saito, S. Machida, T. Terasawa, R. Nakamura, T. Yamamoto, T. Mukai, A. Nishida, and S. Kokubun (1998), Structure and dynamics of magnetic reconnection for substorm onsets with Geotail observations, *J. Geophys. Res.*, *103*, 4419, doi:10.1029/97JA02190.

Nakamura, R., W. Baumjohann, M. Brittnacher, V. A. Sergeev, M. Kubyshkina, T. Mukai, and K. Liou (2001), Flow bursts and auroral activations: Onset timing and foot point location, *J. Geophys. Res.*, *106*, 10,777, doi:10.1029/2000JA000249.

Nishimura, Y., L. R. Lyons, S. Zou, V. Angelopoulos, and S. B. Mende (2010), Substorm triggering by new plasma intrusion: THEMIS all-sky imager observations, *J. Geophys. Res.*, *115*, A07222, doi:10.1029/2009JA015166.

Obuchi, Y., et al. (2008), Initial observations of auroras by the multispectral auroral camera on board the Reimei satellite, *Earth Planets Space*, *60*, 827.

Oguti, T. (1973), Hydrogen emission and electron aurora at the onset of the auroral breakup, *J. Geophys. Res.*, *78*, 7543, doi:10.1029/JA078i031p07543.

Ohtani, S.-I. (2001), Substorm trigger processes in the magnetotail: Recent observations and outstanding issues, *Space Sci. Rev.*, *95*, 347, doi:10.1023/A:1005231122496.

Paschmann, G., S. Haaland, and R. Treumann (Eds.) (2002), *Auroral Plasma Physics*, Springer, New York.

Pontius, D. H., Jr., and R. A. Wolf (1990), Transient flux tubes in the terrestrial magnetosphere, *Geophys. Res. Lett.*, *17*, 49, doi:10.1029/GL017i001p00049.

Pu, Z. Y., A. Korth, Z. X. Chen, R. H. W. Friedel, Q. G. Zong, X. M. Wang, M. H. Hong, S. Y. Fu, Z. X. Liu, and T. I. Pulkkinen (1997), MHD drift ballooning instability near the inner edge of the near-Earth plasma sheet and its application to substorm onset, *J. Geophys. Res.*, *102*, 14,397, doi:10.1029/97JA00772.

Roux, A., S. Perraut, P. Robert, A. Morane, A. Pedersen, A. Korth, G. Kremser, B. Aparicio, D. Rodgers, and R. Pellinen (1991), Plasma sheet instability related to the westward traveling surge, *J. Geophys. Res.*, *96*, 17,697, doi:10.1029/91JA01106.

Saito, H., et al. (2001), INDEX: Piggy-back satellite for aurora observation and technology demonstration, *Acta Astronaut.*, *48*(5–12), 723.

Saito, M. H., Y. Miyashita, M. Fujimoto, I. Shinohara, Y. Saito, K. Liou, and T. Mukai (2008), Ballooning mode waves prior to substorm-associated dipolarizations: Geotail observations, *Geophys. Res. Lett.*, *35*, L07103, doi:10.1029/2008GL033269.

Sakaguchi, K., K. Shiokawa, and E. Donovan (2009), Azimuthal structures of ray auroras at the beginning of auroral substorms, *Geophys. Res. Lett.*, *36*, L23106, doi:10.1029/2009GL041252.

Sakanoi, T., et al. (2003), Development of the multi-spectral auroral camera onboard the index satellite, *Adv. Space Res.*, *32*, 379, doi:10.1016/S0273-1177(03)90276-6.

Samson, J. C., L. R. Lyons, P. T. Newell, F. Creutzberg, and B. Xu (1992), Proton aurora and substorm intensifications, *Geophys. Res. Lett.*, *19*, 2167, doi:10.1029/92GL02184.

Sergeev, V. A. (2002), Ionospheric signatures of magnetospheric particle acceleration in substorms—How to decode them?, in *Proceedings of the 6th International Conference on Substorms*, pp. 39, Univ. of Washington, Seattle.

Sergeev, V. A., V. Angelopoulos, J. T. Gosling, C. A. Cattell, and C. T. Russell (1996), Detection of localized, plasma-depleted flux tubes or bubbles

in the midtail plasma sheet, *J. Geophys. Res.*, *101*, 10,817, doi:10.1029/96JA00460.

Sergeev, V. A., et al. (2000), Multiple-spacecraft observation of a narrow transient plasma jet in the Earth's plasma sheet, *Geophys. Res. Lett.*, *27*, 851, doi:10.1029/1999GL010729.

Shiokawa, K., W. Baumjohann, and G. Haerendel (1997), Braking of high-speed flows in the near-Earth tail, *Geophys. Res. Lett.*, *24*, 1179, doi:10.1029/97GL01062.

Shiokawa, K., K. Yago, K. Yumoto, D. G. Baishev, S. I. Solovyev, F. J. Rich, and S. B. Mende (2005), Ground and satellite observations of substorm onset arcs, *J. Geophys. Res.*, *110*, A12225, doi:10.1029/2005JA011281.

Tsyganenko, N. A. (1995), Modeling the Earth's magnetospheric magnetic field confined within a realistic magnetopause, *J. Geophys. Res.*, *100*, 5599, doi:10.1029/94JA03193.

Uritsky, V. M., J. Liang, E. Donovan, E. Spanswick, D. Knudsen, W. Liu, J. Bonnell, and K. H. Glassmeier (2009), Longitudinally propagating arc wave in the pre-onset optical aurora, *Geophys. Res. Lett.*, *36*, L21103, doi:10.1029/2009GL040777.

Voronkov, I., J. C. Samson, E. Friedrich, R. Rankin, V. T. Tikhonchuk, and E. F. Donovan (2000), On the distinction between, and relevance of, auroral breakup and substorm expansive phase onset, in *Substorms-5, Proceedings of the 5th International Conference on Substorms (ICS-5)*, *Eur. Space Agency Spec. Publ.*, *SP-443*, 249.

Wolf, R. A., Y. Wan, X. Xing, J.-C. Zhang, and S. Sazykin (2009), Entropy and plasma sheet transport, *J. Geophys. Res.*, *114*, A00D05, doi:10.1029/2009JA014044.

Yago, K., K. Shiokawa, K. Hayashi, and K. Yumoto (2005), Auroral particles associated with a substorm brightening arc, *Geophys. Res. Lett.*, *32*, L06104, doi:10.1029/2004GL021894.

Yago, K., K. Shiokawa, K. Yumoto, D. G. Baishev, S. I. Solovyev, and F. J. Rich (2007), Simultaneous DMSP, all-sky camera, and IMAGE FUV observations of the brightening arc at a substorm pseudo-breakup, *Earth Planets Space*, *59*, 45.

Zesta, E., L. R. Lyons, and E. Donovan (2000), The auroral signature of Earthward flow burst observed in the magnetotail, *Geophys. Res. Lett.*, *27*, 3241, doi:10.1029/2000GL000027.

Zesta, E., E. Donovan, L. Lyons, G. Enno, J. S. Murphree, and L. Cogger (2002), The two-dimensional structure of auroral poleward boundary intensifications (PBIs), *J. Geophys. Res.*, *107*(A11), 1350, doi:10.1029/2001JA000260.

Zesta, E., L. Lyons, C.-P. Wang, E. Donovan, H. Frey, and T. Nagai (2006), Auroral poleward boundary intensifications (PBIs): Their two-dimensional structure and associated dynamics in the plasma sheet, *J. Geophys. Res.*, *111*, A05201, doi:10.1029/2004JA010640.

Zhu, P., C. R. Sovinec, C. C. Hegna, A. Bhattacharjee, and K. Germaschewski (2007), Nonlinear ballooning instability in the near-Earth magnetotail: Growth, structure, and possible role in substorms, *J. Geophys. Res.*, *112*, A06222, doi:10.1029/2006JA011991.

Zou, S., L. R. Lyons, C.-P. Wang, A. Boudouridis, J. M. Ruohoniemi, P. C. Anderson, P. L. Dyson, and J. C. Devlin (2009a), On the coupling between the Harang reversal evolution and substorm dynamics: A synthesis of SuperDARN, DMSP, and IMAGE observations, *J. Geophys. Res.*, *114*, A01205, doi:10.1029/2008JA013449.

Zou, S., L. R. Lyons, M. J. Nicolls, C. J. Heinselman, and S. B. Mende (2009b), Nightside ionospheric electrodynamics associated with substorms: PFISR and THEMIS ASI observations, *J. Geophys. Res.*, *114*, A12301, doi:10.1029/2009JA014259.

K. Asamura, Institute of Space and Astronautical Science, 3-1-1 Yoshinodai, Chuo-ku, Sagamihara, Kanagawa 252-5210, Japan.

C. J. Heinselman and M. J. Nicolls, Center for Geospace Studies, SRI International, 333 Ravenswood Ave., Menlo Park, CA 94025, USA.

M. Hirahara, Department of Earth and Planetary Science, University of Tokyo, 7-3-1 Hongo, Bunkyo-ku, Tokyo 113-0033, Japan.

L. R. Lyons and Y. Nishimura, Department of Atmospheric and Oceanic Sciences, University of California, Los Angeles, CA 90095, USA.

Y. Miyashita, Solar-Terrestrial Environment Laboratory, Nagoya University, Furocho, Chikusa, Nagoya 464-8601, Japan.

S. B. Mende, Space Sciences Laboratory, University of California, Berkeley, CA 94720 USA.

M. B. Moldwin and S. Zou, Department of Atmospheric, Oceanic and Space Sciences, University of Michigan, Ann Arbor, MI 48109, USA. (shashaz@umich.edu)

T. Sakanoi, Planetary Plasma and Atmospheric Research Center, Tohoku University, 28 Kawauchi, Aoba-ku, Sendai 980-8576, Japan.